



HAL
open science

Self-regulation in tip growth: The role of cell wall ageing

Eelco Eggen, M. Niels de Keijzer, Bela M. Mulder

► **To cite this version:**

Eelco Eggen, M. Niels de Keijzer, Bela M. Mulder. Self-regulation in tip growth: The role of cell wall ageing. *Journal of Theoretical Biology*, 2011, 283 (1), pp.113. 10.1016/j.jtbi.2011.05.034 . hal-00719491

HAL Id: hal-00719491

<https://hal.science/hal-00719491>

Submitted on 20 Jul 2012

HAL is a multi-disciplinary open access archive for the deposit and dissemination of scientific research documents, whether they are published or not. The documents may come from teaching and research institutions in France or abroad, or from public or private research centers.

L'archive ouverte pluridisciplinaire **HAL**, est destinée au dépôt et à la diffusion de documents scientifiques de niveau recherche, publiés ou non, émanant des établissements d'enseignement et de recherche français ou étrangers, des laboratoires publics ou privés.

Author's Accepted Manuscript

Self-regulation in tip growth: The role of cell wall ageing

Eelco Eggen, M. Niels de Keijzer, Bela M. Mulder

PII: S0022-5193(11)00286-4
DOI: doi:10.1016/j.jtbi.2011.05.034
Reference: YJTBI6498

To appear in: *Journal of Theoretical Biology*

Received date: 13 October 2010
Revised date: 13 May 2011
Accepted date: 27 May 2011

Cite this article as: Eelco Eggen, M. Niels de Keijzer and Bela M. Mulder, Self-regulation in tip growth: The role of cell wall ageing, *Journal of Theoretical Biology*, doi:[10.1016/j.jtbi.2011.05.034](https://doi.org/10.1016/j.jtbi.2011.05.034)

This is a PDF file of an unedited manuscript that has been accepted for publication. As a service to our customers we are providing this early version of the manuscript. The manuscript will undergo copyediting, typesetting, and review of the resulting galley proof before it is published in its final citable form. Please note that during the production process errors may be discovered which could affect the content, and all legal disclaimers that apply to the journal pertain.



www.elsevier.com/locate/jtbi

Self-regulation in tip growth: the role of cell wall ageing

Eelco Eggen^a, M. Niels de Keijzer^b, Bela M. Mulder^b

^a*Institute for Theoretical Physics, Utrecht University, Leuvenlaan 4, 3584 CE Utrecht, The Netherlands*

^b*FOM-Institute AMOLF, Science Park 104, 1098 XG Amsterdam, The Netherlands*

Abstract

We develop a model to describe the effect of cell wall ageing on the local expansion rate of tip growing cells. Starting from an exact equation for the stationary age-distribution of the wall material, we propose a generic measure for the local expansion propensity of the wall if the ageing process is described by a constant rate Poissonian decay process. This ageing process may be either interpreted as biochemical in nature describing the finite lifetime of regulatory proteins, or as mechanical in nature describing the gradual “hardening” of the wall through cross-linking or gelation of the wall polymers. In this way we can construct models for tip-growth in which material deposition, evolving wall properties and surface expansion are self-consistently intertwined. As a proof of principle, we implement our ageing approach in two different idealized models of tip-growth, obtaining the stationary tip shapes as a function of the ageing parameter. In the first, the spatial distribution of delivery of growth material is determined by the local curvature of the cell and the growth mode is orthogonal. In the second, the growth material originates from a Vesicle Supply Center, a point-like representation of the Spitzenkörper as found in fungal hyphae, and the growth mode is isometric.

Keywords: tip growth; modelling; self-regulation; morphogenesis

1. Introduction

Tip growth, the localized extension of walled cells at just one of their ends leading to a filamentous cell morphology, occurs in algae, fungi and higher plants (for an overview see Geitmann et al., 2001). This unique growth morphology is exploited by various organisms e.g. in reproduction (pollen tubes

in plants, fungal hyphae) and for surface-area enhancement and mechanical anchoring (root hairs in plants). At first sight, tip growth seems to be a beguilingly simple example of biological morphogenesis: In general both growth velocity and tip shape remain approximately constant over time and in the absence of additional spatial cues the cell shape has cylindrical symmetry. In reality, it is quite a complex dynamical process which, first of all, involves the intracellular production of vesicles containing wall-building materials, the transport and localized delivery of these vesicles to the site of growth, where they subsequently undergo exocytosis, simultaneously adding phospholipids to the plasma membrane and depositing their contents to the nascent cell wall.

Reinhardt (1892), in one of the first papers that attempted to model tip growth, already concluded that the material properties of the cell wall over the apical region could not be homogeneous. He argued that the newly delivered material right at the tip should be easily deformable to allow for extensional growth, while the material farther from the tip should effectively rigidify to resist further expansion in the radial direction. Indeed, over the past few years a number of papers have appeared that recognize that a proper mechanical description of growth must involve the notion of a gradient in material properties over the apical region (Goriely and Tabor, 2003a,b; Dumais et al., 2006; Fayant et al., 2010). In these approaches, however, this gradient is at the outset chosen to have a fixed, usually phenomenologically motivated, functional form. Almost two decades ago, Koch (1982), however, was the first to suggest that tip growth is possibly homeostatically controlled by a feedback mechanism whereby the local material state of the wall controls the local rate of incorporation of new material. Although his so-called “soft spot” hypothesis (see also Koch (1994)) rests on, with hindsight, physically and biologically shaky foundations, the idea by itself that there is feedback on the growth process due to some form of intrinsic dynamics of the wall material is plausible. In fact, the gradient of mechanical properties over the apical region must be the result of the interplay between the intrinsic wall dynamics and the growth process.

As far as we are aware, however, to date no attempt was made to self-consistently include the intrinsic dynamics of the cell wall into the description of tip-growth. Here we formulate a generic model to account for the feedback of an *ageing process* of the wall material, whatever its precise microscopic origin, on the local expansion rate of tip-growing cells, showing that it leads to an additional level of self-organisation of the tip-growth process. We start by

formulating an explicit model for the space-time evolution of the age distribution of the wall material during the growth process, and derive the equation that determines its form in steady state. We assume that the ageing process is well described by constant rate Poissonian decay process, describing either the finite life-time of co-deposited regulatory factors, or the on-going physico/chemical cross-linking of the wall polymers. On this basis we derive a phenomenological quantity that locally describes the “propensity” of the nascent wall to expand, given the availability of new growth material. We then show that this approach leads to analytically or numerically tractable models of tip growth that allow the systematic exploration of the influence of wall ageing on tip morphologies.

The outline of the paper is as follows: In Section 2 we introduce the geometrical setting of our tip growth model. In Section 3 we discuss the two main regulatory factors that determine the growth process, the so-called expansion propensity, which determines the rate at which locally available growth material contributes to growth, and the supply factor which describes the spatial dependence of the available material. In Section 4 we then present the application of our framework to two specific examples of simple models of tip growth, a purely geometrical model and a classical model for fungal hyphae. After the discussion in Section 5, a number of appendices collect some of the more technical details.

2. Geometrical setting

2.1. Surface shape

We assume that the tip-growing cell is in a stationary state. In this state growth proceeds at a constant velocity v , and while individual material points on the cell surface are undergoing a continuous dynamics, the shape of the cell as a whole is unchanged, apart from an overall translation in space in the direction of growth. Assuming the stationary shape is cylindrically symmetric, we can parametrize it through

$$\mathbf{r}(s, \varphi) = (\rho(s) \cos \varphi, \rho(s) \sin \varphi, z(s)), \quad (1)$$

where s is the arclength from the apex along a meridional section of the cell, φ is an azimuthal angle around the symmetry-axis, ρ the radial distance from the symmetry-axis to the surface, and z a coordinate along the symmetry axis. The unit vector normal to the surface is given by

$$\hat{\mathbf{n}}(s, \varphi) = (-z'(s) \cos \varphi, -z'(s) \sin \varphi, \rho'(s)). \quad (2)$$

where the prime throughout denotes differentiation with respect to s . If we define ψ as the angle between the surface normal and the positive z -axis we have

$$\cos \psi = \rho'(s), \quad (3)$$

$$\sin \psi = -z'(s). \quad (4)$$

The position of the apex is given by

$$\rho(0) = 0,$$

$$z(0) = z_0,$$

where z_0 can be freely chosen to fix the origin of the reference frame along the axis of symmetry. This geometrical setting is illustrated in Figure 1.

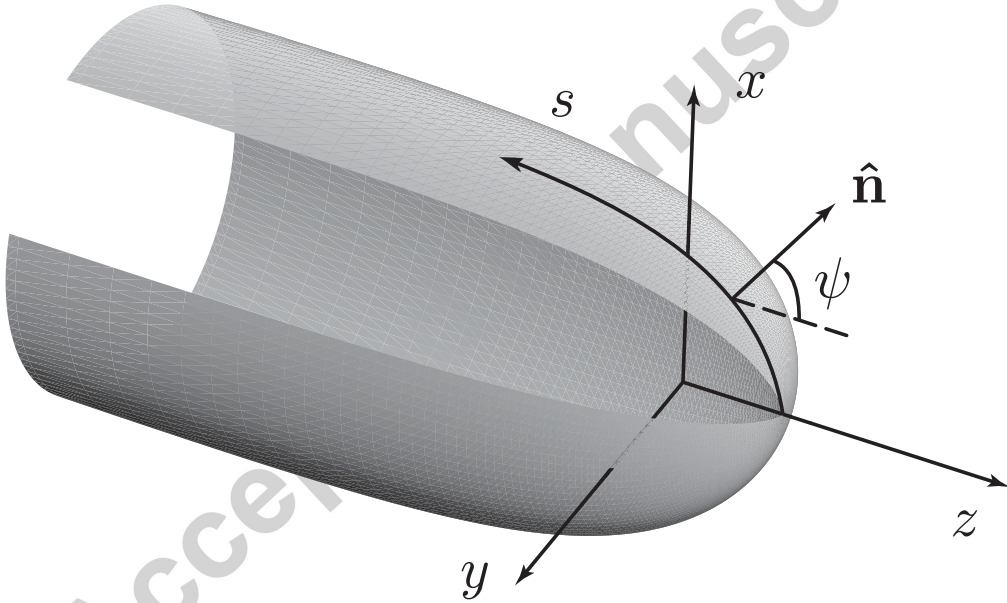


Figure 1: Coordinate system for describing stationary tip growth.

We further assume that the tip is smooth at the apex and consequently,

$$\rho'(0) = 1,$$

$$z'(0) = 0,$$

and that as the distance to the apex becomes large, the shape tends to a cylinder with a constant radius

$$\begin{aligned}\lim_{s \rightarrow \infty} \rho(s) &= R, \\ \lim_{s \rightarrow \infty} \rho'(s) &= 0.\end{aligned}$$

The infinitesimal element of surface area of the cell is simply given by

$$dA(s, \varphi) = \rho(s) ds d\varphi. \quad (5)$$

Finally, an important quantity characterizing the local properties of the surface is the mean curvature, which, in terms of our parametrization, is given by

$$H(s) = \frac{1}{2} \left(\frac{\sqrt{1 - \rho'(s)^2}}{\rho(s)} - \frac{\rho''(s)}{\sqrt{1 - \rho'(s)^2}} \right). \quad (6)$$

We refer the reader to Appendix A for the relevant details.

2.2. Surface expansion

The growth process causes the surface to expand, but because of the anisometric tip shape this expansion rate is not constant over the surface. We define the local expansion rate $\Phi(s)$ as the increase of surface area per unit of existing area at a point a distance s away from the apex. In order for a stationary state to exist, where the apex moves with the constant growth velocity v , the local expansion rate must vanish as $s \rightarrow \infty$.

For a co-moving observer the surface expansion reveals itself as a motion of material points within the surface in the direction pointing away from the apex. This flow speed of the material points again depends on the distance from the tip and is denoted by $v(s)$. Clearly, $\lim_{s \rightarrow \infty} v(s) = v$. In Appendix B we derive the following relationship between the local expansion rate and the flow speed:

$$\rho(s)\Phi(s) = \frac{d(\rho(s)v(s))}{ds} = \rho'(s)v(s) + \rho(s)v'(s) \quad (7)$$

To obtain the rate at which the surface area of an ‘‘apical cap’’, i.e. a part of the surface bounded by a longitudinal circle and containing the apex, increases, we integrate (7) over the appropriate area yielding

$$\dot{A}(s) = \int_0^s \rho(s) ds \int_0^{2\pi} d\phi \Phi(s) = 2\pi \int_0^s ds \frac{d(\rho(s)v(s))}{ds} = 2\pi \rho(s)v(s). \quad (8)$$

Letting $s \rightarrow \infty$ we find the expected result that total surface area increases as $\dot{A}_{\text{tot}} = 2\pi Rv$, where $R = \rho(\infty)$ is the final cell radius. This latter result illustrates how the stationary tip growing cell can keep its shape constant by effectively adding a cylindrical segment of area infinitely far away from the apex.

2.3. Growth mode

A three dimensional surface growth process is not fully specified by the local areal expansion rate $\Phi(s)$ alone. Generically, an initially circular infinitesimal element of surface area at time t will expand under the growth process into a shape that an infinitesimal time dt later is well approximated by an ellipse. Only the surface area of this ellipse $\propto a \times b$, where a and b are the length of the minor and major axes respectively, is fixed by the local areal expansion rate. The aspect ratio of the ellipse, i.e. the ratio b/a of the lengths of the axes, still needs to be determined. This quantity follows from the components of the rate of strain tensor (B.9) as derived in Appendix B. The orientation of the ellipse, however, is fixed by our assumption of cylindrical symmetry, which constrains the axes of the ellipse to lie along the meridional and azimuthal directions respectively. To give a realistic account of the full growth dynamics clearly requires considering the mechanical properties of the cell wall, which currently is an active area of research (see e.g. Goriely and Tabor (2003a); Dumais et al. (2006); Campàs and Mahadevan (2009); Fayant et al. (2010)). However, this is beyond the scope of the current work, which focusses on the generic aspects of wall ageing on the overall expansion rate. In the illustrative examples presented in Section 4 we therefore limit ourselves to two geometrical models of growth that have been discussed in previous modelling efforts (Gierz and Bartnicki-García, 2001). Both growth modes, either implicitly or explicitly, fix the ratio of the diagonal elements of the rate of strain tensor. For the relevant derivations we refer the reader to Appendix C.

The first growth mode we consider requires the motion of material points to be always perpendicular to the surface, yielding so-called *orthogonal growth*. This growth mode has in the past been suggested to be in accord with experimental observations (Bartnicki-García et al., 2000) and is at the same time simply stated geometrically. In orthogonal growth both the flow speed of material points

$$v(s) = -vz'(s) \quad (9)$$

and the local expansion rate

$$\Phi(s) = 2v\rho'(s)H(s) \quad (10)$$

are fully fixed by the geometry of the surface alone.

In the second growth mode we consider, the local element of surface area expands isotropically during growth, yielding so-called *isometric growth*. Although experiments have shown that in most cases filamentous growth displays clear strain anisotropies (Castle (1958); Chen (1973); Kataoka (1982); Dumais et al. (2004)), this growth mode has the advantage of greatly simplifying both the derivation of the shape equations as well as their numerical analysis. In isometric growth the flow speed is given by

$$v(s) = \frac{v}{R}\rho(s), \quad (11)$$

and the local expansion rate

$$\Phi(s) = 2\frac{v}{R}\rho'(s). \quad (12)$$

3. Regulation of expansion

We assume that the local rate of areal expansion the cell of is regulated by two distinct factors. The first is obviously the availability of new wall-building material which is delivered by intracellular mechanisms to specific location. We model this by a position dependent rate of delivery of material $g(s)$ we call the *supply factor*. The second factor represents the regulatory influence of the material state of the cell wall on the degree to which the available wall material is actually used to contribute to expansion. In the simplest possible realization of this notion we model these effects through a multiplicative factor $f(s)$, which we term the *expansion propensity*. With these assumptions we write

$$\Phi(s) \propto f(s)g(s). \quad (13)$$

Below we address both the modelling of these two factors separately, but not before first considering the age distribution of the wall material.

3.1. Age distribution of wall material

Our basic assumption on the expansion propensity is that it depends only on the local properties of the existing wall material. These properties will in principle change over time, as the growth process is constantly altering the cell wall composition, due to the absorption of new wall building material and its subsequent ageing. In order to describe these ageing effects in the cell wall, we must give a description of the time elapsed since the incorporation of a certain portion of wall material. Therefore, each position on the cell surface is characterized by an age distribution defined as follows: $\Psi(\tau, s)d\tau$ is the fraction of wall material at position s that has spent a time between τ and $\tau + d\tau$ as a part of the wall. This distribution is normalized, such that

$$\int_0^{\infty} \Psi(\tau, s)d\tau = 1. \quad (14)$$

Given that we have a stationary growth process, the age distribution itself is time independent. This means that it is invariant under a set of transformations representing the growth dynamics. We can distinguish four processes due to the growth dynamics in the cell wall that affect the age distribution. First of all there is the intrinsic *ageing* process itself: with the passage of time physical and chemical processes cause changes in the material state of the wall. Then there are two kinematic effects due to the growth process: *flow*, the motion of material points away from the apex as the surface expands, and *dilution*, the same material is spread out over a larger area due to the expansion. Finally, there is *rejuvenation*, as new material is incorporated. These four processes are illustrated in Figure 2.

We now consider a cohort of material points in small area $\Delta A(t)$ centered on a point at distance s from the apex, with ages between τ and $\tau + \Delta\tau$. Under the action of the growth process during an infinitesimal time dt this cohort will now occupy a slighter larger area $\Delta A(t+dt) = (1+\Phi(s)dt)\Delta A(t) + \mathcal{O}(dt^2)$, effectively ‘diluting’ the (surface) concentration. The area occupied by the cohort is now centered on $s + v(s)dt + \mathcal{O}(dt^2)$ due to the flow, and the ages of the cohort now range from $\tau + dt$ to $\tau + dt + \Delta\tau$ due to the ageing process. In the steady state the local age distribution does not change over time and hence we require that to first order in dt

$$\Psi(\tau + dt, s + v(s)dt)\Delta A(t + dt)\Delta\tau = \Psi(\tau, s)\Delta A(t)\Delta\tau \quad (15)$$

Expanding the left hand side to first order in dt , subtracting the right hand side, and canceling all common factors, then yields a first order PDE for the

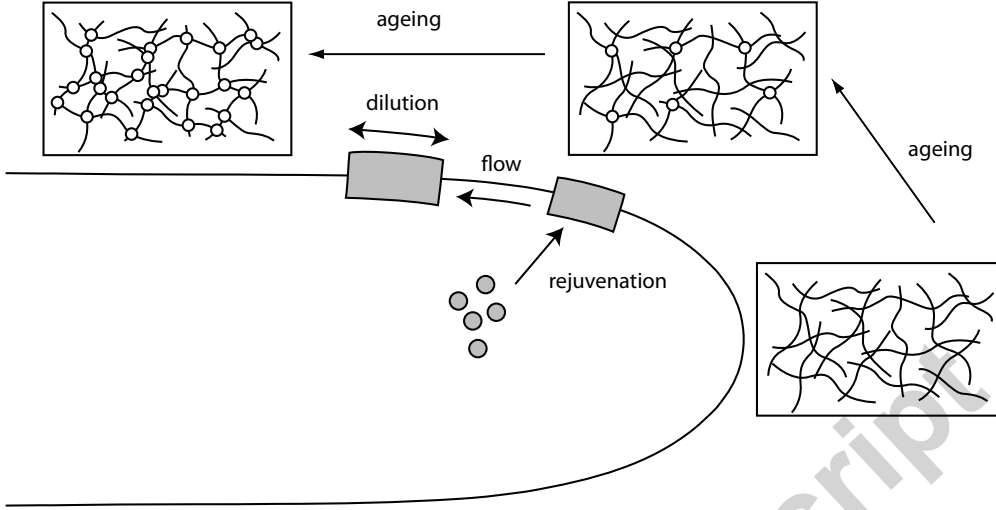


Figure 2: Illustration of the four dynamic effects of cell wall growth: ageing, here conceived as increasing cross-linking between the wall polymers, flow, dilution and rejuvenation .

age distribution

$$\frac{\partial \Psi(\tau, s)}{\partial \tau} + v(s) \frac{\partial \Psi(\tau, s)}{\partial s} + \Phi(s) \Psi(\tau, s) = 0 \quad (16)$$

which is analogous to the well-known McKendrick- von Foerster equation describing the dynamics of age-structured populations in theoretical ecology (Kot, 2001, see e.g.), here, however, with a position dependent spatial drift term and a dilution effect, due to the surface expansion.

Finally, the continuous influx of new material rejuvenates the age distribution. We assume that the amount of matter added per unit area per unit time is proportional to the increase in area. Then, the fractional increase in area in an infinitesimal time interval $\propto \Phi(s)dt$ must be equal to fraction of material $\propto \Psi(0, s)dt$ younger than dt , and hence we are led to the boundary condition

$$\Psi(0, s) = \Phi(s). \quad (17)$$

In principle, for given functions $v(s)$ and $\Phi(s)$, this linear first order PDE can be solved by the using the method of characteristics. The line of initial value points $\{(0, s) | s \in [0, \infty)\}$ is a sufficient set of boundary points for this problem, as the tangent vector to the characteristics is given by $(1, v(s))$,

where $0 \leq v(s) \leq v$, and hence never tangent to the initial value curve. In the following, however, we do not solve this equation directly, but rather an integral transform of it, whose boundary condition is explicitly derived.

3.2. The expansion propensity

We now need to address how the expansion propensity depends on the age distribution of the wall material. Here we make the assumption that there is a single Poissonian process with which the contribution to the propensity to expand of a given amount of wall material decays with increasing age. With this definition we set

$$f(s) = \int_0^\infty d\tau \Psi(\tau, s) e^{-\alpha\tau}, \quad (18)$$

where α is the *ageing rate*. In the limiting case $\alpha = 0$ (no ageing) the expansion propensity is normalized to unity, whereas as required it vanishes for $\alpha \rightarrow \infty$ (very fast ageing).

A few candidates for such an ageing process have already been discussed in the literature. One proposed mechanism for the regulation of cell wall deposition in tip growth (for a recent review see Cárdenas, 2009) is through the fact that calcium ions are required to lower the energy barrier for vesicle fusion at the plasma membrane. The influx of these ions into the cell is effected by calcium channels. These channels in turn are deposited into the membrane through exocytosis. If we now assume that to a first approximation the incorporation rate is proportional to the local calcium concentration, itself taken to be proportional to the ion-channel density, and that the active channels have an exponentially distributed lifetime, we have a first example of such a Poissonian ageing process. Another example is the increasing stiffening of the cell wall due to the ongoing de-esterification of pectins under the action of co-deposited pectin methylesterases (Fayant et al., 2010). If these enzymes are present in abundance, and the rate of cleavage per methyl group is constant, one expects an exponential decay of the number of uncleaved methyl groups per amount of pectin as a function of time after insertion. As the de-esterified groups can cross-link using calcium ions as linkers causing the pectins to gel, we can in a very rough approximation posit that the expansion propensity is proportional to the mean number of surviving methyl groups. The latter approximation is essentially equivalent to the so-called “soft spot” hypothesis, originally proposed by Koch (1994). This hypothesis stated that

the increasing degree of cross-linking of wall polymers with time since deposition (illustrated in Figure 3) would physically prevent the incorporation of new wall material. For a constant cross-linking rate one would again find that the available number of cross-linking sites per unit amount of material decreases exponentially with age. Although obviously highly simplistic, this hypothesis does provide a concrete metaphor to illustrate our otherwise fairly generic ageing mechanism.

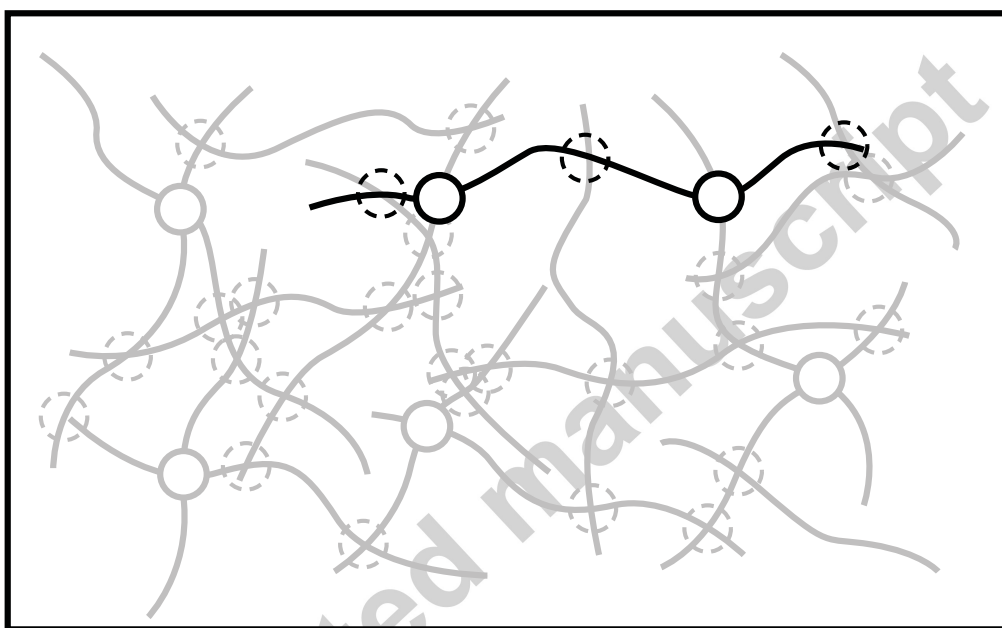


Figure 3: Illustration of the concept of cell wall ageing. The highlighted polymer has five locations where cross-linkers can bind, of which two are occupied.

Combining the definition (18) with the equation for the age distribution (16), and using (17), we arrive at a one-dimensional initial value problem for the expansion propensity $f(s)$

$$v(s)f'(s) + (\Phi(s) + \alpha)f(s) = \Phi(s), \quad (19)$$

To obtain a boundary condition, we consider the limit $s \rightarrow 0$ of the expression (7) for the local expansion rate, which shows that for a smooth tip the flow speed $v(0) = 0$ vanishes at the apex. Using this in (19) evaluated at $s = 0$

then yields

$$f(0) = \frac{\Phi(0)}{\Phi(0) + \alpha}. \quad (20)$$

In order for the uptake propensity to be a proper autonomous regulator of tip growth, we require that it vanishes as $s \rightarrow \infty$. As the expansion rate also vanishes in this limit, this requires that the two terms on the left hand side of (19) must balance each other asymptotically, i.e.

$$v \lim_{s \rightarrow \infty} \frac{f'(s)}{f(s)} = \lim_{s \rightarrow \infty} \frac{\Phi(s)}{f(s)} - \alpha \leq 0. \quad (21)$$

Further on we will make use of an equivalent integral formulation for the evolution of the expansion propensity. We arrive at this formulation by rearranging (19), eliminating $\Phi(s)$ using (7) and multiplying by $\rho(s)$

$$\alpha \rho(s) f(s) = (\rho(s) v(s))' (1 - f(s)) - \rho(s) v(s) f'(s) = (\rho(s) v(s) (1 - f(s)))' \quad (22)$$

Integration then yields

$$\alpha \int_0^s ds' \rho(s') f(s') = \rho(s) v(s) (1 - f(s)), \quad (23)$$

and specially its useful limiting case (cf. (8))

$$\int_0^\infty ds \rho(s) f(s) = \frac{Rv}{\alpha}. \quad (24)$$

3.3. Supply factor

How much wall-building material is delivered to a certain location could in principle depend on all the details of the intracellular processes involved in the delivery of vesicles to the plasma membrane. From a formal perspective within our framework, however, the only constraint on the supply factor comes from the requirement that the expansion propensity vanishes for $s \rightarrow \infty$ (Eq. (21)). Indeed, if, without loss of generality, we choose

$$\Phi(s) = \frac{\Phi(0)}{f(0) g(0)} f(s) g(s) = (\Phi(0) + \alpha) f(s) \frac{g(s)}{g(0)} \quad (25)$$

then, because of the limit (21),

$$\lim_{s \rightarrow \infty} \frac{g(s)}{g(0)} \leq \frac{\alpha}{\Phi(0) + \alpha} = 1 - f(0). \quad (26)$$

This constraint rules out the potentially simplest choice $g(s) = g(0)$, i.e. a constant delivery rate independent of the position, as this is only compatible with the limit of infinite fast ageing, $\alpha \rightarrow \infty$, in which case Eq. (19) yields $f(s) = f(0) = 0$.

Arguably, a physically realistic description of the supply factor should involve the active transport and/or the diffusion of vesicles in the volume of the cell, with the local rate of exocytosis playing the role of a flux-type boundary conditions. We ourselves have pursued such an approach in the context of fungal growth in earlier work (Tindemans et al., 2006). For the examples in Section 4 we again limit ourselves to two specific and highly simplified choices for the supply factor, both of which have been discussed in the literature. These choices for the supply factor have the advantage of being much simpler from a computational perspective, yet retain many of the essential features of tip-focussed vesicle delivery.

The first was already suggested by Goriely et al. (2005), and assumes that the delivery rate is solely dependent on the local curvature of the surface

$$g(s) = H(s) \quad (27)$$

This choice ignores all details of the delivery process, but achieves focussed delivery by assuming more supply at the more strongly curved areas on the surface. The second choice, appropriate to the case of tip growing fungi, is the assumption that the wall material is delivered by vesicles that reach the cell surface by ballistic transport after their release from a “Spitzenkörper”, here represented as a point-like Vesicle Supply Center (VSC), as it was introduced by Gierz and Bartnicki-García (2001). In this case the supply factor is given by

$$g(s) \propto \begin{cases} \text{The flux of additional surface material delivered to an} \\ \text{element of cell surface at position } s \text{ by a point source} \\ \text{located at the origin.} \end{cases} \quad (28)$$

and achieves focussing by projecting more vesicles per unit area to regions closer to the VSC, i.e. the apical region, than areas farther away along the tube. Finally, it should be mentioned that there is strong experimental evidence that in several tip-growing cells the maximum rate of vesicle delivery is *not* at the apex, but rather at an annular region just downstream from the apex (Bove et al., 2008; Zonia and Munnik, 2008). This could in principle be modelled by a non-monotonic supply factor, with a maximum at an apex distance $s_{max} > 0$, but we chose to forego these additional complexities here.

4. Application to specific examples of growth models

4.1. Curvature-driven delivery

In our first model, we take the supply function $g(s)$ to be proportional to the mean surface curvature $H(s)$, and we employ the orthogonal growth mode. One hand, by the definition (25), we then have

$$\frac{\Phi(s)}{\Phi(0)} = \frac{f(s) H(s)}{f(0) H(0)}. \quad (29)$$

On the other hand, the orthogonal growth condition (10) implies

$$\frac{\Phi(s)}{\Phi(0)} = \frac{\rho'(s)H(s)}{\rho'(0)H(0)} = \rho'(s) \frac{H(s)}{H(0)}. \quad (30)$$

Combining these two identities, then yields a direct relationship between the shape of the cell and the expansion propensity,

$$\frac{f(s)}{f(0)} = \rho'(s). \quad (31)$$

If we insert this expression into the condition (24), we fix the apical value of the expansion propensity

$$f(0) = \frac{2v}{\alpha R}. \quad (32)$$

Combining this result with the boundary condition (20) and the orthogonal growth prescription we obtain

$$RH(0) = \frac{\kappa}{\kappa - 2}, \text{ where } \kappa = \alpha R/v. \quad (33)$$

Note that this uniquely determines the curvature of the tip at the apex as a function of the ageing rate, the final radius and the growth velocity. Also, this relation tells us that we here we must require $\kappa > 2$ in order to have a finite tip curvature.

Equation (23) can now be rewritten as a first-order nonlinear ordinary differential equation for $\rho(s)$

$$\rho(s) = R\sqrt{1 - \rho'(s)^2} \left(1 - \frac{2}{\kappa} \rho'(s) \right). \quad (34)$$

Parametrizing all shape functions in terms of the angle ψ between the surface normal and the z -axis, enables us to solve the problem explicitly, yielding

$$\rho(\psi) = R \sin \psi \left(1 - \frac{2}{\kappa} \cos \psi \right), \quad (35)$$

$$z(\psi) = z_0 - R \left[1 - \cos \psi - \frac{2}{\kappa} (\sin^2 \psi + \log \cos \psi) \right], \quad (36)$$

$$s(\psi) = R \left[\psi + \frac{2}{\kappa} \left(\log \frac{1 + \sin \psi}{\cos \psi} - 2 \sin \psi \right) \right]. \quad (37)$$

The resulting solutions for several values of κ are shown in Figure 4.



Figure 4: Calculated shapes for the simple geometrical model. Values for the dimensionless ageing parameter κ are 2.02 (lower left), 4 (middle) and 202 (upper right).

It is interesting to note that the slow growth/fast ageing limit ($\kappa \rightarrow \infty$) of this solution yields the extremely simple form

$$\rho_{\infty}(\psi) = R \sin \psi, \quad (38)$$

$$z_{\infty}(\psi) = z_0 - R(1 - \cos \psi), \quad (39)$$

$$s_{\infty}(\psi) = R\psi. \quad (40)$$

for $\psi \leq \pi/2$, i.e. a hemispherical cap, which can be continued into an arbitrarily long cylinder of radius R . Intriguingly, a 2D version of such a solution was already found in the early simulations by van Batenburg et al. (1986) of a tip growth model where the orthogonal expansion rate of the surface was assumed to decrease linearly with the axial distance to the tip. Indeed, here we find that in terms of this distance $\Delta z = z_0 - z_\infty(\psi)$ the uptake propensity is given by

$$f_\infty(\Delta z) = \begin{cases} f_\infty(0) \left(1 - \frac{\Delta z}{R}\right) & \Delta z \leq R \\ 0 & \Delta z > R \end{cases}, \quad (41)$$

whilst the curvature $H_\infty(\Delta z) = 1/R$ is constant for $\Delta z \leq R$, implying the full identity of these models in this limit.

4.2. The VSC model

In the VSC model we position an isotropic, constant-rate source of growth material at the origin of our coordinate frame. The appropriate supply factor can then be derived by making the rate of growth material impinging on a patch of cell surface area proportional to the solid angle subtended by this patch as seen from the VSC. This yields

$$g(s) \propto \frac{\mathbf{r}(s) \cdot \hat{\mathbf{n}}(s)}{|\mathbf{r}(s)|^3} = \frac{z(s)\rho'(s) - z'(s)\rho(s)}{(\rho^2(s) + z^2(s))^{\frac{3}{2}}}. \quad (42)$$

For this application we choose the isometric growth mode, which through Eq. (12) also expresses the local expansion rate in terms of the geometry. Using the normalization Eq. (25) also allows us to express the expansion propensity in terms of the surface geometry

$$f(s) = \frac{\Phi(s)}{(\Phi(0) + \alpha)} \frac{g(0)}{g(s)} = \frac{1}{z^2(0)} \frac{2}{(2 + \kappa)} \frac{\rho'(s) (\rho^2(s) + z^2(s))^{\frac{3}{2}}}{(z(s)\rho'(s) - z'(s)\rho(s))}. \quad (43)$$

Inserting these expressions into the steady-state equation for the expansion propensity then yields a single closed form second order differential equation involving $\rho(s)$, $z(s)$ and their derivatives. Using the parametrization Eq. (3), the dependency between $\rho(s)$ and $z(s)$ can be resolved, finally yielding a set of two coupled first order equations, which we show in full in (D.6) and (D.7). Note that these equations contain the as yet undetermined quantity $z(0)$, i.e. the distance between the VSC and the apex of the cell. This quantity can be determined self-consistently from the solutions to the equations, when the

ultimate cell radius R is considered as fixed. In practice this is done using a standard “shooting approach”, which is described in Appendix D. In Figure 5 we show the computed tip shapes for a number of different ageing rates. These results show that, while the shape itself only becomes slightly more “blunt” at higher ageing rates, the tip–VSC distance does increase markedly on the ageing rate.

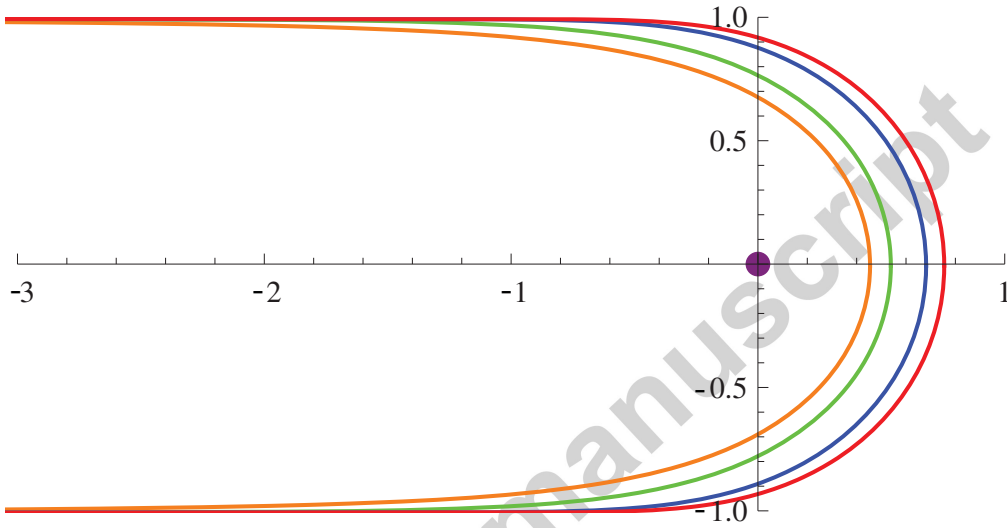


Figure 5: The shape of the tip in the VSC-model for different values of the ageing parameter κ with distances measured in units of the tube diameter R , and using the location of the VSC (filled disk) as origin. From the *innermost* to the *outermost* shape κ ranges through 0 (orange), 1 (green), 5 (blue), 10 (red). Faster ageing tips are blunter, and have a larger apex-VSC distance.

Finally, in Figure 6 we plot the expansion propensity $f(s)$ for different values of the ageing rate, showing that as ageing increases the region where growth is possible becomes limited to the area close to the apex.

5. Discussion and outlook

We have presented what are arguably the first, albeit simplified, models of tip growth that self-consistently couple material deposition, evolving wall properties and growth. This additional mechanism significantly enlarges the dynamical phase space of growth models. To date most models essentially only involve a single timescale related to the growth rate, $t_{\text{growth}} = R/v$,

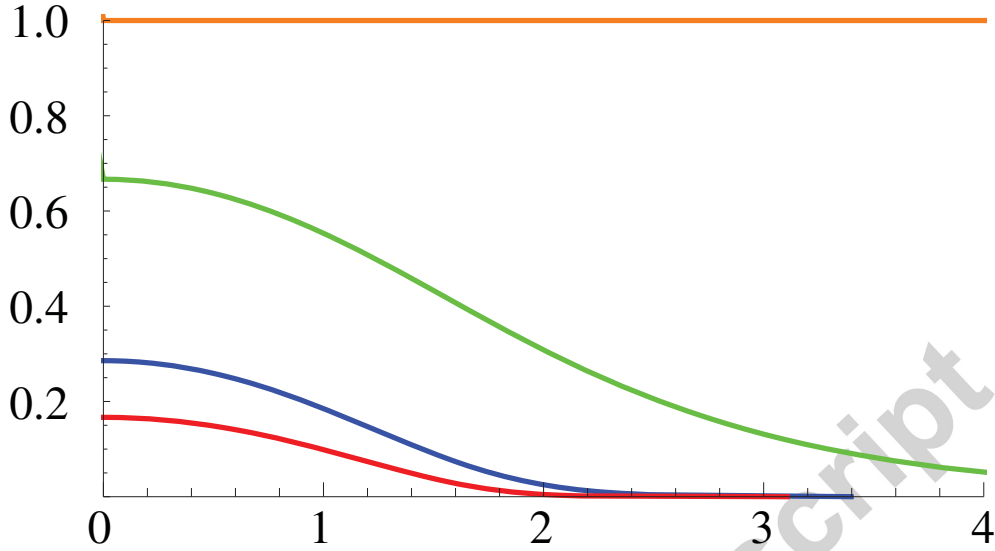


Figure 6: The expansion propensity $f(s)$ plotted as a function of the distance from the apex measured in units of the tube radius R . From the *outermost* to the *innermost* shape, κ ranges through 0 (orange), 1 (green), 5 (blue), 10 (red). With increasing rate of ageing the region where growth is possible shrinks to an area close to the apex.

which is readily observable at the global scale. In the ageing approach, a new timescale, t_{ageing} , appears, which is associated with the intrinsic dynamics of the newly deposited wall material, and hence more difficult to observe. It is the interplay between these two timescales that allows the new class of models to account for a much wider variety of tip-shapes than hitherto possible, as illustrated e.g. in Figure 2.

A key assumption in our model is the generic notion of a feedback of the local material state of the wall on the propensity to expand in surface area, given that enough wall building material is available. We have obviously chosen a very generic functional form for this feedback, allowing only a phenomenological interpretation at this stage. Our underlying dynamics of the age distribution of the cell wall material, could, however, serve as the basis for more detailed microscopic ageing mechanisms. From an experimental point of view, it is obviously very challenging to probe the dynamical processes going on in the nascent cell wall. Nevertheless, we may hope that a combination of micromechanical (see e.g. Zerzour et al., 2009) and biochemical (see e.g. Fayant et al., 2010) measurements that probe the local properties of the

wall with quantitative measurement on the local rate of exocytosis (see e.g. Zonia and Munnik, 2008) may serve to validate some of the ideas presented here.

What is still clearly lacking from our model is the true physics of growth and expansion, which requires the application of the principles of continuum mechanics (for a nice recent review see Goriely and Tabor, 2008), coupled to perhaps more realistic microscopic models of the developing cell wall. Goriely and Tabor (2003a,b) and later Dumais et al. (2006) have already formulated models in which the mechanics is explicitly taken into account. However, these models essentially impose a stationary gradient of mechanical properties along the growing tip, rather than having this gradient emerge self-consistently on the basis of the combined process of material incorporation, ageing and extension. By combining the approach of our present work which with the explicit use of elasticity theory, by having the relevant mechanical constants depend explicitly on the “age” of the wall material, one can hope to achieve a synthesis which is reasonable both from a biological as well as physical point of view. We are currently working to formulate such a model.

Acknowledgements. This work is part of the research program of the “Stichting voor Fundamenteel Onderzoek der Materie (FOM)”, which is financially supported by the “Nederlandse Organisatie voor Wetenschappelijk Onderzoek (NWO)”. The work of NdK is made possible by grant no. 05DOP04 from the NWO-FOM programme “Dynamics of Patterns”.

Appendix A. The geometry of axisymmetric surfaces

In this Appendix, and the two following ones, we give a very concise overview of the differential geometry of surfaces relevant to the problem of tip-growth. Readers interested in more background are urged to consult a reference on the geometry surfaces such as Carmo (1976) and a primer on tensors such as Joshi (1995).

Consider a parameterization of a tip-shaped axisymmetric surface using the variables (σ, φ) , where σ is an arbitrary parameter along the meridional direction and φ is the usual azimuthal (cylindrical) angle. Because of the axial symmetry, the shape of the surface is fully described by the functions $\rho(\sigma)$ and $z(\sigma)$. The arc length from the apex to σ is then defined by

$$s(\sigma) \equiv \int_{\sigma_0}^{\sigma} d\sigma' \sqrt{\rho'(\sigma')^2 + z'(\sigma')^2}, \quad (\text{A.1})$$

where $\sigma = \sigma_0$ denotes the position of the apex. It is convenient to choose the arc length s itself as the meridional parameter, as already done in the main text. From the definition of the arc length it follows that

$$\rho'(s)^2 + z'(s)^2 = 1. \quad (\text{A.2})$$

This relationship implies that the surface shape can essentially be described solely by the function $\rho(s)$. However, we also use $z(s)$ for notational simplicity. Using Eq. (A.2), we can solve for $z(s)$

$$z'(s) = -\sqrt{1 - \rho'(s)^2}, \quad (\text{A.3})$$

$$z(s) = z(0) - \int_0^s ds' \sqrt{1 - \rho'(s')^2}. \quad (\text{A.4})$$

The negative root is chosen for the derivative of $z(s)$ because we have defined the positive z -axis in the direction of growth, so that the surface itself evolves towards the negative z -axis and, hence, $z(0)$ is the maximum of $z(s)$. We note that the function $z(s)$, and more specifically its starting value $z(0)$, is of significance only if there is a preferred location of the origin, such as a vesicle supply center.

We use Eq. (1) to define the cell surface, parameterized by s and φ . Locally, the geometry of this surface is characterized by the set of basis vectors which span the plane tangential to the surface

$$\mathbf{r}_s \equiv \partial_s \mathbf{r} = (\rho'(s) \cos(\varphi), \rho'(s) \sin(\varphi), z'(s)), \quad (\text{A.5})$$

$$\mathbf{r}_\varphi \equiv \partial_\varphi \mathbf{r} = (-\rho(s) \sin(\varphi), \rho(s) \cos(\varphi), 0). \quad (\text{A.6})$$

Note that in this parametrization $\mathbf{r}_s \cdot \mathbf{r}_s = 1$. The outward normal unit vector $\hat{\mathbf{n}}(s, \varphi)$ on the surface, already presented in Eq. (2) is determined from the definition

$$\hat{\mathbf{n}}(s, \varphi) = \frac{\mathbf{r}_s \times \mathbf{r}_\varphi}{|\mathbf{r}_s \times \mathbf{r}_\varphi|}. \quad (\text{A.7})$$

For the further development, we need a few more geometrical quantities related to the surface. The first is the metric tensor

$$g_{\mu\nu} \equiv \mathbf{r}_\mu \cdot \mathbf{r}_\nu = \begin{pmatrix} 1 & 0 \\ 0 & \rho(s)^2 \end{pmatrix}. \quad (\text{A.8})$$

where the Greek indices run over s and φ respectively. Note that the off-diagonal zeroes mean that $\{\mathbf{r}_s, \mathbf{r}_\varphi\}$ form an orthogonal basis. This metric

tensor has an inverse denoted by

$$g^{\mu\nu} = \begin{pmatrix} 1 & 0 \\ 0 & \rho(s)^{-2} \end{pmatrix}. \quad (\text{A.9})$$

Given an arbitrary (covariant) tensor $T_{\mu\nu}$ we use $g^{\mu\nu}$ to “raise” an index and obtain the mixed form that allows us to calculate invariants, such as the trace which is defined through

$$\text{Tr}(T) = g^{\mu\nu} T_{\nu\mu} \equiv T^\mu{}_\mu, \quad (\text{A.10})$$

where we employ the Einstein summation convention. Next, we calculate the curvature tensor

$$k_{\mu\nu} \equiv \partial_\mu \hat{\mathbf{n}} \cdot \mathbf{r}_\nu = \begin{pmatrix} \frac{-\rho''(s)}{\sqrt{1-\rho'(s)^2}} & 0 \\ 0 & \rho(s)\sqrt{1-\rho'(s)^2} \end{pmatrix}. \quad (\text{A.11})$$

The curvature tensor can be used to calculate the two invariant scalar curvatures, the *extrinsic* (mean) curvature and the *intrinsic* (Gaussian) curvature of the surface. The mean curvature is given by

$$\begin{aligned} H(s) &= \frac{1}{2} \text{Tr}(k^\mu{}_\nu) = \frac{1}{2} k^\mu{}_\mu = \frac{1}{2} g^{\mu\nu} k_{\mu\nu} \\ &= \frac{1}{2} \left(\frac{-\rho''(s)}{\sqrt{1-\rho'(s)^2}} + \frac{\sqrt{1-\rho'(s)^2}}{\rho(s)} \right), \end{aligned} \quad (\text{A.12})$$

and the Gaussian curvature is given by

$$K(s) = \det(k^\mu{}_\nu) = \eta_{\mu\nu} k^\mu{}_\nu = -\frac{\rho''(s)}{\rho(s)}, \quad (\text{A.13})$$

where $\eta_{\mu\nu}$ is the rank-two Levi-Cevita tensor. Finally we note that the element of surface area is given by

$$dA(s, \varphi) = \sqrt{(\mathbf{r}_s \times \mathbf{r}_\varphi) \cdot (\mathbf{r}_s \times \mathbf{r}_\varphi)} ds d\varphi = \sqrt{\det(g_{\mu\nu})} ds d\varphi = \rho(s) ds d\varphi. \quad (\text{A.14})$$

Appendix B. Surface deformations and growth

In order to describe surface deformations and growth we first introduce the notion of a material point. At an arbitrary initial $t = 0$ such a point is, up to a rotation around the z -axis, uniquely identified by its distance from the tip s_0 . In the co-moving frame the distance to the tip of this material will increase, which we describe by the function $S(t)$ with $S(0) = s_0$. Because of the assumed axisymmetry the motion of this point will be purely meridional, so that the azimuthal angle φ is constant. The flow velocity of the material point in the co-moving frame is therefore given by

$$\mathbf{V}(t) = \frac{dS(t)}{dt} \mathbf{r}_s(S(t), \varphi). \quad (\text{B.1})$$

In the steady state these quantities no longer depend explicitly on time and we can write

$$\mathbf{V}(s, \varphi) = v(s) \mathbf{r}_s(s, \varphi), \quad (\text{B.2})$$

which defines the flow speed used in the main text. To obtain the track, $\mathbf{X}(t|\mathbf{r}(s_0, \varphi))$ with $X(0|\mathbf{r}(s_0, \varphi)) = \mathbf{r}(s_0, \varphi)$, of the material point in the space-fixed laboratory frame, it suffices to realize that in the steady state the tip as a whole by definition simply shifts with a constant velocity in the direction of the symmetry axis, so that

$$\mathbf{X}(t|\mathbf{r}(s_0, \varphi)) = \mathbf{r}(S(t), \varphi) + vt\hat{\mathbf{z}}, \quad (\text{B.3})$$

where $\hat{\mathbf{z}}$ is the unit vector in the positive z -direction. The time derivative of this quantity yields the velocity of the material points at a certain position

$$\mathbf{u}(s, \varphi) = \left. \frac{d\mathbf{X}(t|\mathbf{r}(s_0, \varphi))}{dt} \right|_{S(t)=s} = v(s) \mathbf{r}_s(s, \varphi) + v\hat{\mathbf{z}}. \quad (\text{B.4})$$

The components of this vector in a local frame are given by

$$u^s = \mathbf{u}(s, \varphi) \cdot \mathbf{r}_s(s, \varphi) = v(s) + vz'(s), \quad (\text{B.5})$$

$$u^\varphi \propto \mathbf{u}(s, \varphi) \cdot \mathbf{r}_\varphi(s, \varphi) = 0, \quad (\text{B.6})$$

$$u^\perp = \mathbf{u}(s, \varphi) \cdot \hat{\mathbf{n}}(s, \varphi) = v\rho'(s). \quad (\text{B.7})$$

The surface deformation induces a change in the metric of the surface, which defines the rate of strain tensor

$$\begin{aligned} \dot{\epsilon}_{\mu\nu} &= \frac{1}{2} \frac{dg_{\mu\nu}}{dt} = \frac{1}{2} \frac{d}{dt} [\partial_\mu \mathbf{X}(t|\mathbf{r}(s_0, \varphi)) \cdot \partial_\nu \mathbf{X}(t|\mathbf{r}(s_0, \varphi))]_{S(t)=s} \\ &= \frac{1}{2} \{ \mathbf{r}_\mu \cdot \partial_\nu \mathbf{u} + \mathbf{r}_\nu \cdot \partial_\mu \mathbf{u} \}. \end{aligned} \quad (\text{B.8})$$

In our parametrization the rate of strain tensor takes the explicit form

$$\dot{\varepsilon}_{\mu\nu} = \begin{pmatrix} v'(s) & 0 \\ 0 & \rho(s) \rho'(s) v(s) \end{pmatrix} \quad (\text{B.9})$$

The relative expansion rate of the surface can now be considered from its definition

$$\Phi(s) = \frac{1}{dA(s, \varphi)} \frac{d}{dt} dA(s, \varphi) = \frac{1}{\sqrt{\det(g_{\mu\nu})}} \frac{d}{dt} \sqrt{\det(g_{\mu\nu})}. \quad (\text{B.10})$$

The time derivative involved is readily calculated from the Jacobi formula for the derivative of the determinant of an invertible matrix

$$\frac{d}{dx} \det A(x) = \det A(x) \text{Tr} \left(A(x)^{-1} \frac{d}{dx} A(x) \right), \quad (\text{B.11})$$

yielding

$$\frac{d}{dt} \sqrt{\det(g_{\mu\nu})} = \sqrt{\det(g_{\mu\nu})} \text{Tr} \left(g^{\mu\sigma} \frac{1}{2} \frac{d}{dt} g_{\sigma\nu} \right) = \sqrt{\det(g_{\mu\nu})} \text{Tr}(\dot{\varepsilon}^{\mu}_{\nu}), \quad (\text{B.12})$$

so that

$$\Phi(s) = \text{Tr}(\dot{\varepsilon}^{\mu}_{\nu}) = \frac{\rho'(s)v(s)}{\rho(s)} + v'(s) = \frac{1}{\rho(s)} \frac{d(\rho(s)v(s))}{ds}. \quad (\text{B.13})$$

Appendix C. The growth modes

In the orthogonal growth mode the meridional velocity component of growth Eq. (B.5) vanishes, yielding

$$v(s) = -vz'(s), \quad (\text{C.1})$$

and the velocity of material points is given by

$$\mathbf{u} = u^{\perp} \hat{\mathbf{n}}. \quad (\text{C.2})$$

We now note that in this case

$$\mathbf{r}_{\nu} \cdot \partial_{\mu} \mathbf{u} = \mathbf{r}_{\nu} \cdot \partial_{\mu} (u^{\perp} \hat{\mathbf{n}}) = \partial_{\mu} u^{\perp} (\mathbf{r}_{\nu} \cdot \hat{\mathbf{n}}) + u^{\perp} (\mathbf{r}_{\nu} \cdot \partial_{\mu} \hat{\mathbf{n}}) = u^{\perp} (\mathbf{r}_{\nu} \cdot \partial_{\mu} \hat{\mathbf{n}}), \quad (\text{C.3})$$

so that

$$\dot{\varepsilon}_{\mu\nu} = u^\perp k_{\mu\nu}, \quad (\text{C.4})$$

where we have used the symmetry of $k_{\mu\nu}$. We therefore have

$$\Phi(s) = \text{Tr}(\dot{\varepsilon}_{\mu\nu}^{\mu}) = u^\perp \text{Tr}(k_{\mu\nu}^{\mu}) = 2v\rho'(s)H(s). \quad (\text{C.5})$$

In the isometric growth rate, the two components of the mixed index rate of strain tensor $\dot{\varepsilon}_{\mu\nu}^{\mu}$ (cf. Eq. (B.9)) are equal, so that

$$v'(s) = \frac{v(s)}{\rho(s)}\rho'(s). \quad (\text{C.6})$$

This implies that $v(s)$ and $\rho(s)$ are proportional, where the proportionality constant is readily found by considering $v(\infty) = v$ and $\rho(\infty) = R$. This yields the flow velocity

$$v(s) = \frac{v}{R}\rho(s), \quad (\text{C.7})$$

and the local expansion rate

$$\Phi(s) = \text{Tr}(\dot{\varepsilon}_{\mu\nu}^{\mu}) = 2\frac{v(s)}{\rho(s)}\rho'(s) = 2\frac{v}{R}\rho'(s). \quad (\text{C.8})$$

Appendix D. The isometric VSC model

In order to formulate the equations for the isometric growth VSC model it is useful to introduce dimensionless quantities through the adoption of R as a unit of length and R/v as a unit of time. With this prescription we have

$$\Phi(s) = 2\rho'(s), \quad (\text{D.1})$$

and

$$f(s) = F_0 \frac{\rho'(s)(\rho^2(s) + z^2(s))^{\frac{3}{2}}}{[z(s)\rho'(s) - z'(s)\rho(s)]}, \quad (\text{D.2})$$

where $F_0 = 2/[(2 + \kappa)z^2(0)]$ and the dimensionless ageing rate κ was introduced in Section 4.1. Inserting this into the steady state equation for the expansion propensity Eq. (19) yields

$$\begin{aligned} F_0 \sqrt{\rho(s)^2 + z(s)^2} \{ & \rho'(s) [\rho'(s)z(s) - \rho(s)z'(s)] \times \\ & [\rho(s)^2 (5\rho'(s) + \kappa) + 3\rho(s)z(s)z'(s) + z(s)^2 (2\rho'(s) + \kappa)] \\ & + \rho(s)^2 [\rho(s)^2 + z(s)^2] (\rho'(s)z''(s) - z'(s)\rho''(s)) \} \\ & - 2\rho'(s) [\rho'(s)z(s) - \rho(s)z'(s)]^2 = 0. \end{aligned} \quad (\text{D.3})$$

Note that $z(s)$ and $\rho(s)$ are related through $z'(s) = -\sqrt{1 - \rho'(s)^2}$, so that

$$z''(s) = \frac{\rho'(s)\rho''(s)}{\sqrt{1 - \rho'(s)^2}}. \quad (\text{D.4})$$

By introducing the angle ψ (cf. Eq. (3)) as a dependent variable, we can switch to ρ as our independent variable. We readily find

$$\frac{d\psi}{d\rho} = \frac{\rho''(s)}{\rho'(s)z'(s)}, \quad (\text{D.5})$$

$$\frac{dz}{d\rho} = \frac{z'(s)}{\rho'(s)} = -\tan \psi. \quad (\text{D.6})$$

Inserting these into Eq. (D.3) and simplifying yields

$$\begin{aligned} & F_0 \sqrt{\rho^2 + z^2(\rho)} \{ [\rho \sin \psi(\rho) + z(\rho) \cos \psi(\rho)] \\ & \quad \times [\rho^2(5 \cos \psi(\rho) + \kappa) - 3\rho z(\rho) \sin \psi(\rho) + z^2(\rho)(2 \cos \psi(\rho) + \kappa)] \\ & \quad - \rho^2[\rho^2 + z^2(\rho)]\psi'(\rho) \} \\ & \quad - 2[\rho \sin \psi(\rho) + z(\rho) \cos \psi(\rho)]^2 = 0. \end{aligned} \quad (\text{D.7})$$

This last equation needs to be solved in conjunction with Eq. (D.6) under the boundary conditions

$$\psi(0) = 0, \quad (\text{D.8})$$

$$z(0) = \sqrt{\frac{2}{(2 + \kappa)F_0}}, \quad (\text{D.9})$$

$$\psi(1) = \frac{\pi}{2}, \quad (\text{D.10})$$

$$z(1) = -\infty. \quad (\text{D.11})$$

Note that both the equation (D.7) and the boundary condition for $z(0)$ actually contain the as yet undetermined amplitude F_0 . The latter, however, can be replaced with the known condition $z'(0) = 0$. The resulting set equations is amenable to a shooting approach (see e.g. Press et al., 2007, Chapter 18), which solves the two point boundary value problem by turning into an initial value problem, where a subset of initial conditions at one point is varied until the boundary conditions at the other point are met. In our case we vary $z(0)$, through changing F_0 , and $\psi'(0)$. For each choice we solve the initial value problem using a standard PDE solver (Mathematica's `NDSolve`), and then use a tailor-made root-finding algorithm to adjust the free parameters until the boundary conditions at infinity are met.

References

- Bartnicki-García, S., Bracker, C.E., Gierz, G., López-Franco, R., Lu, H., 2000. Mapping the growth of fungal hyphae: orthogonal cell wall expansion during tip growth and the role of turgor. *Biophys. J.* 79, 2382–2390.
- van Batenburg, F.H.D., Jonker, R., Kijne, J.W., 1986. *Rhizobium* induces marked root hair curling by redirection of tip growth: a computer simulation. *Physiol. Plant.* 66, 476–480.
- Bove, J., Vaillancourt, B., Kroeger, J., Hepler, P.K., Wiseman, P.W., Geitmann, A., 2008. Magnitude and direction of vesicle dynamics in growing pollen tubes using spatiotemporal image correlation spectroscopy and fluorescence recovery after photobleaching. *Plant physiology* 147, 1646–58.
- Campàs, O., Mahadevan, L., 2009. Shape and dynamics of tip-growing cells. *Current biology* : CB 19, 2102–7.
- Cárdenas, L., 2009. New findings in the mechanisms regulating polar growth in root hair cells. *Plant Signaling & Behavior* 4, 4–8.
- Carmo, M.D., 1976. *Differential Geometry of Curves and Surfaces*. Prentice Hall.
- Castle, E.S., 1958. The topography of tip growth in a plant cell. *J. Gen. Physiol.* 41, 913–926.
- Chen, J.C.W., 1973. The kinetics of tip growth in the *Nitella* rhizoid. *Plant Cell Physiol.* 14, 631–640.
- Dumais, J., Long, S.R., Shaw, S.L., 2004. The mechanics of surface expansion anisotropy in *Medicago truncatula* root hairs. *Plant physiology* 136, 3266–75.
- Dumais, J., Shaw, S.L., Steele, C.R., Long, S.R., Ray, P.M., 2006. An anisotropic-viscoplastic model of plant cell morphogenesis by tip growth. *The International journal of developmental biology* 50, 209–22.
- Fayant, P., Girlanda, O., Chebli, Y., Aubin, C.E., Villemure, I., Geitmann, A., 2010. Finite element model of polar growth in pollen tubes. *The Plant cell* 22, 2579–93.

- Geitmann, A., Cresti, M., Heath, I.B. (Eds.), 2001. Cell biology of plant and fungal tip growth. volume Vol. 328 of *NATO ASI series. Series I :Life and Behavioural Sciences*, IOS Press, Amsterdam.
- Gierz, G., Bartnicki-García, S., 2001. A three-dimensional model of fungal morphogenesis based on the vesicle supply center concept. *J. theor. Biol.* 208, 151–164.
- Goriely, A., Károlyi, G., Tabor, M., 2005. Growth induced curve dynamics for filamentary micro-organisms. *J. Math. Biol.* 51, 355–366.
- Goriely, A., Tabor, M., 2003a. Biomechanical models of hyphal tip growth in actinomycetes. *J. theor. Biol.* 222, 211–218.
- Goriely, A., Tabor, M., 2003b. Self-similar tip growth in filamentary organisms. *Phys. Rev. Lett.* 90, 108101.
- Goriely, A., Tabor, M., 2008. Mathematical modeling of hyphal tip growth. *Fungal Biol. Rev.* 22, 77–83.
- Joshi, A.W., 1995. *Matrices and Tensors in Physics*. Wiley-Interscience. 3d edition.
- Kataoka, H., 1982. Colchicine-induced expansion of *Vaucheria* cell apex. Alteration from isotropic to transversally anisotropic growth.
- Koch, A.L., 1982. The shape of the hyphal tips of fungi. *J. Gen. Microbiol.* 128, 947–951.
- Koch, A.L., 1994. The problem of hyphal growth in streptomycetes and fungi. *J. theor. Biol.* 171, 137–150.
- Kot, M., 2001. *Elements of mathematical ecology*. Cambridge University Press.
- Press, W.H., Teukolsky, S.A., Vetterling, W.T., Flannery, B.P., 2007. *Numerical Recipes in C: The Art of Scientific Computing*. Cambridge University Press, New York, NY, USA. 3d edition.
- Reinhardt, M.O., 1892. Das wachstum der pilzhyphen. *Jahrb. Wissenschaft Bot.* 23, 479–566.

- Tindemans, S.H., Kern, N., Mulder, B.M., 2006. The diffusive vesicle supply center model for tip growth in fungal hyphae. *Journal of theoretical biology* 238, 937–48.
- Zerzour, R., Kroeger, J., Geitmann, A., 2009. Polar growth in pollen tubes is associated with spatially confined dynamic changes in cell mechanical properties. *Dev. Biol.* 334, 437–46.
- Zonia, L., Munnik, T., 2008. Vesicle trafficking dynamics and visualization of zones of exocytosis and endocytosis in tobacco pollen tubes. *Journal of experimental botany* 59, 861–73.

Accepted manuscript

- We model the role of cell wall ageing in tip growing cells.
- We derive an equation for the age distribution of the wall building material.
- We define a generic feedback mechanism which regulates cell expansion based on this age distribution.
- We show that our approach leads to rich class of tractable models of tip growth.

Accepted manuscript